Energy scales in $4f^1$ delafossite magnets: crystal-field splittings larger than the strength of spin-orbit coupling in KCeO$_2$

M. S. Eldeeb,[1] T. Petersen,[1] L. Hozoi,[1] V. Yushankhai,[2,3] and U. K. Rößler[1]

[1]*Institute for Theoretical Solid State Physics, Leibniz IFW Dresden, Helmholtzstr. 20, 01069 Dresden, Germany*
[2]*Joint Institute for Nuclear Research, Joliot-Curie 6, 141980 Dubna, Russia*
[3]*Max-Planck-Institut für Physik komplexer Systeme, Nöthnitzerstr. 38, 01187 Dresden, Germany*
(Dated: December 25, 2021)

Ytterbium-based delafossites with effective $\tilde{S} = 1/2$ moments are intensively investigated as candidates for quantum spin-liquid ground states. While the synthesis of related cerium compounds has also been reported, many important details concerning their crystal, electronic, and magnetic structures are unclear. Here we analyze the $\tilde{S} = 1/2$ system KCeO$_2$, combining complementary theoretical methods. The lattice geometry was optimized and the band structure investigated using density functional theory extended to the level of a GGA+U calculation in order to reproduce the correct insulating behavior. The Ce $4f^1$ states were then analysed in more detail with the help of *ab initio* wave-function-based computations. Unusually large effective crystal-field splittings of up to 320 meV are predicted, which puts KCeO$_2$ in the strong field coupling regime. Our results reveal a subtle interplay between ligand-cage electrostatics and the trigonal field generated by the extended crystalline surroundings, relevant in the context of recent studies on tunning the nature of the ground-state wave-function in $4f$ triangular-lattice and pyrochlore compounds. It also makes KCeO$_2$ an interesting model system in relation to the effect of large crystal-field splittings on the anisotropy of intersite exchange in spin-orbit coupled quantum magnets.

Introduction. Along with the on-site Coulomb repulsion, spin-orbit coupling is considered to define a dominant energy scale in f-electron compounds. In $4f^{13}$ ytterbium oxides and chalcogenides, for example, materials that are investigated intensively nowadays as candidates for spin-liquid ground states [1–8], the separation between the low-lying states of the split $J = 7/2$ ground-state multiplet and those of the excited $J = 5/2$ term is in the range of 1.3 eV. Comparatively, the splittings induced by the ionic solid-state surroundings imply a scale of tens of meV [3–9]. A notable feature, however, is that for lighter ligands in these systems, i. e., O instead of S or Se, the crystal-field splittings may increase up to $\approx$100 meV [5–7, 9]. This can be qualitatively explained by having shorter M-O bonds, which leads to stronger ligand-field effects, and also by more subtle chemical aspects giving rise to stronger trigonal compression of the oxygen cage in the oxides. Starting from such observations on the Yb-based compounds, in particular, the triangular-lattice NaYbL$_2$ delafossites [3–9], the Ce-based analogues, e. g., KCeO$_2$ [10], look from an electronic-structure point of view somewhat more peculiar: the Ce $4f$ states are known to be more extended, i. e., likely more sensitive to the ligand environment; on the other hand, the spin-orbit coupling is significantly weaker for early rare-earth ions, by factors of $\sim$5 for Ce^{3+} as compared to Yb^{3+} [11]. An interesting regime can then be realized where spin-orbit interactions and crystal-field splittings have similar magnitude. Situations of this kind were discussed in the context of strong deviations from the $j_{\text{eff}} = 1/2$ picture in t_{2g}^5 $5d$ and $4d$ quantum magnets such as CaIrO$_3$ [12, 13] and α-RuCl$_3$ under high pressure [14], where the trigonal splittings imply a larger energy scale as compared to

the strength of the $5d/4d$-shell spin-orbit coupling; they modify the nature of the ground-state wave-functions and therefore the relevant intersite exchange paths. Looking for related physics in the case of $4f$ materials, we address in this study the on-site electronic structure of Ce ions in KCeO$_2$. Impetus is also provided by recently finding crystal-field splittings of up to 125 meV in the sister compound KCeS$_2$ [15].

Lattice geometry and electronic structure from density functional theory. While the synthesis of KCeO$_2$ was already reported decades ago [10], a complete characterization of its crystal structure is still missing. We therefore start our discussion with an analysis of structural aspects in KCeO$_2$ — for clarifying those we rely on density-functional calculations with periodic boundary conditions. KCeO$_2$ crystallizes in the NaFeO$_2$-type delafossite structure with a rhombohedral lattice (space group $R\bar{3}m$, no 166). In hexagonal setting K, Ce, and O have the Wyckoff positions $3a$ $(0,0,0)$, $3b$ $(0,0,1/2)$, and $6c$ $(0,0,z)$, respectively (see Fig. 1). The experimental room-temperature lattice constants are $a = 3.66$ and $c = 18.66$ Å [10]. The position of O in the cell, i. e., the z parameter, has not yet been established. Using the delafossite setting, we determined this parameter and also performed a complete lattice optimization. The full-potential local-orbital code FPLO (version 18) [16] was employed for this purpose. As exchange-correlation functional we applied the generalized-gradient approximation (GGA) [17]. In the context of lattice optimization for $4f$ compounds, details on the performance of FPLO and of different functionals were recently published by Majumder *et al.* [18].

We first optimized the z parameter using the experi-

mentally derived lattice constants and three different approaches: plain GGA with and without spin polarization and also a GGA+U spin-split calculation. For the latter, the Coulomb repulsion parameter was set to $U = 5.0$ eV and the Hund exchange to $J_H = 0.69$ eV by fixing the Slater parameters for the $4f$ states of Ce to $F_0 = U$, $F_2 = 8.54$, $F_4 = 5.37$, and $F_6 = 3.86$ eV. The F_2 to F_6 ratio was adopted from Hartree-Fock calculations for free ions [19]; the value of J_H was renormalized by a factor of 0.7. The so-called atomic limit was used as double-counting correction. A k-mesh of $24 \times 24 \times 24$ points, corresponding to 13824 irreducible k points, was found to be sufficiently accurate.

Results based on density functional theory (DFT) are listed in Table I. The data show that accounting for spin polarization has only marginal influence on the lattice geometry and also that the GGA+U scheme modifies the z parameter by only a small amount. Plain GGA yields a metallic state as Ce $4f$ bands show up at the Fermi level. On the other hand, in subsequent GGA+U calculations a finite gap arises. The density of states for the three different approaches are compared in Fig. 2.

The optimization of the lattice parameters at the GGA+U level yields a too large lattice volume, by about 3.5% as compared to experimental estimates [10]. This matches the usual tendency of the GGA functional to overestimate both volume and spin polarization. The cohesive energy of the compound is largely determined
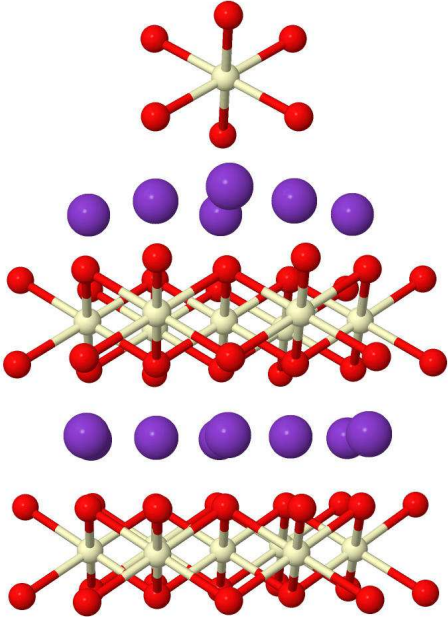

FIG. 1. Successive ionic layers in KCeO$_2$. Light yellow, red, and purple spheres represent Ce, O, and K sites, respectively. For the top CeO$_2$ layer, only one single CeO$_6$ octahedron is displayed.
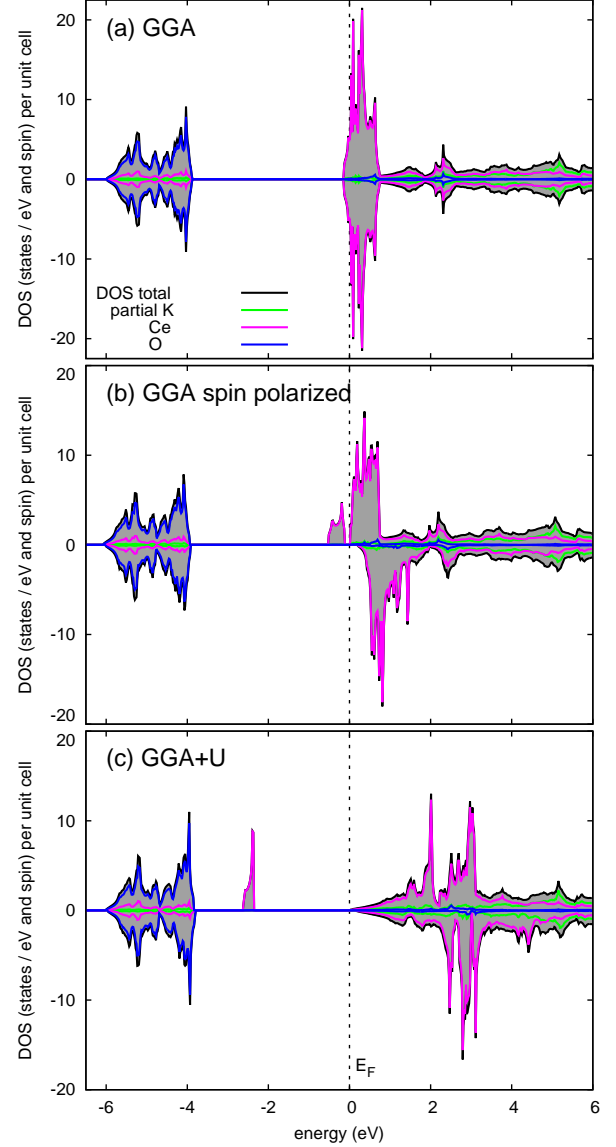

FIG. 2. Densities of states (DOS's) in KCeO$_2$ from DFT, including site projected DOS's for the three different ionic species: results for spin-degenerate (a) and spin-polarized (b) plain GGA along with (c) GGA+U data. Spin-majority and minority DOS's are plotted in positive and negative ordinate direction, the Fermi level E_F is at zero energy.

by the ionic contribution. The electronic states of Ce, in particular, the $5d$'s, and their hybridization with O states do play a certain role and an improved accuracy probably requires improved description of electronic correlations. Yet, the relatively small effect on the O-ion position in the different DFT schemes suggests that the geometry optimization is reasonably robust and can be reliably used for a more detailed analysis of the Ce $4f$ electronic structure. The value computed by DFT for the O-ion z-axis fractional coordinate implies rather strong

trigonal compression of the ligand cages, with O-Ce-O angles deviating by 7.7° from 90° bond angles. The impact of this trigonal distortion on the $4f$-shell energy level structure is discussed in the next section. For the quantum chemical calculations, we adopted the O z-axis parameter derived by GGA+U when using the experimental lattice constants.

Quantum chemical calculations for the Ce^{3+} $4f^1$ multiplet structure. In the intermediate coupling regime with equally strong spin-orbit and crystal-field interactions, for describing the energy levels and the corresponding eigenstates of the $4f^1$ configuration of Ce^{3+}, the full basis of 14 atomic-like spin orbitals should be used. Besides the value of the spin-orbit coupling λ, for D_{3d} point-group symmetry [10], six crystal-field parameters are required in the relevant effective model [20]. Fitting those effective interaction constants require rather detailed experimental data — f-f excitation energies, g factors etc. The situation becomes delicate when not all f-f transitions are captured in, e.g., the neutron scattering spectra [4] or additional peaks arise due to vacancies, interstitials, or strong electron-phonon couplings [15, 21].

The associated uncertainties, however, can be overcome with the help of *ab initio* computations of the $4f$ multiplet structure. Using crystallographic data as on the third position in Table I, we performed such calculations for a finite set of atoms having a CeO_6 unit as central region, in particular, multiconfiguration and multireference quantum-chemical computations [22] both with and without spin-orbit coupling, and the main results are reported in Table II. An active space defined by the seven Ce $4f$ orbitals was employed to this end for the initial multiconfiguration calculation. The latter was carried out as a complete-active-space self-consistent-field (CASSCF) optimization [22] for an average of the seven $4f^1$ $S=1/2$ states. Multireference configuration-interaction (MRCI) wave-functions were subsequently built by additionally considering single and double excitations [23] out of the Ce $4f$ and O $2p$ orbitals of the

TABLE I. Structural data obtained for $KCeO_2$ by various types of DFT computations. For the first four entries the experiental lattice constants were used. Both scalar relativistic and fully relativistic calculations with spin-orbit coupling (SOC) were performed.

Method	a (Å)	c (Å)	z
GGA			0.2301
GGA spin polarized	3.66^a	18.66^a	0.2304
GGA+U spin polarized			0.2310
GGA+U+SOC			0.2311
GGA+U spin polarized	3.694	18.964	0.2299
GGA+U+SOC	3.696	18.954	0.2299

^{a} Fixed.

TABLE II. Ce^{3+} $4f^1$ multiplet structure (relative energies in meV) using fractional coordinates as optimized by DFT (see text), CASSCF and MRCI data without spin-orbit coupling along with spin-orbit MRCI results (MRCI+SOC). For the double group, notations as in Ref. [34] (e.g., Appendix I in [34]) are used. The ground-state g factors are $g_c = 0.31$ and $g_{ab} = 0.09$.

	CASSCF	MRCI	MRCI+SOC	
$^2A_{2u}$	0	0	0	Γ_6
^2E_u	91	96	121	$\Gamma_4+\Gamma_5$
	91	96	143	Γ_6
$^2A_{1u}$	132	131	252	Γ_6
$^2E'_u$	226	229	352	$\Gamma_4+\Gamma_5$
	226	229	395	Γ_6
$^2A'_{2u}$	314	318	469	Γ_6

'central' CeO_6 octahedron. Effective core potentials and valence basis sets as optimized in Refs. [24, 25] were used for the central Ce ion, along with all-electron [$4s3p2d$] Douglas-Kroll basis sets for the adjacent ligands [26]. To model the charge distribution in the immediate vicinity, we relied on large-core pseudopotentials including the $4f$ electrons in the core as concerns the six Ce nearest neighbors [27, 28] and on total-ion potentials as concerns the twelve adjacent K sites [29]. The remaining part of the extended crystalline surroundings was modeled as an effective electrostatic field [30]. To determine the symmetries of the spin-orbit states, we computed the g factors for each of those and additionally the dipole transition matrix elements for $4f{\rightarrow}5d$ excitations. For instance, the $4f^1$ spin-orbit states of $\Gamma_4+\Gamma_5$ symmetry can be quickly identified as those which have z-component dipole matrix elements [where z (c) coincides with the trigonal axis] with only two of the $5d^1$ spin-orbit states [31]. Larger active orbital spaces including both shells, $4f$ and $5d$, were used for obtaining the dipole transition matrix elements. The g factors were obtained according to the procedure described in Ref. [32]; by symmetry, the g_{ab} components vanish for the $\Gamma_4+\Gamma_5$ spin-orbit states. The quantum chemical package MOLPRO [33] was employed for all wave-function-based computations.

In the absence of spin-orbit interactions, an octahedral ligand field with full cubic symmetry splits the f levels into three sets, a_{2u}, t_{2u}, and t_{1u}, each of the latter two being triply degenerate. The a_{2u} orbital has its lobes normal to the facets of the ligand octahedral cage and therefore the lowest energy because the Coulomb repulsion with electronic charge at the ligand sites is minimized; the t_{1u} orbitals, on the other hand, point directly toward the ligands and are of highest energy [35]. Since the smallest energy scale is defined by the a_{2u}–t_{2u} splitting [36], the a_{2u} and t_{2u} contributions to the ground-state spin-orbit wave-function do not differ by much for cubic octahedral environment of the Ce ion [37]. Lowering the $4f$-site symmetry to trigonal (D_{3d} symmetry

in the delafossite structure), the three-fold degeneracy of the t_{2u} and t_{1u} states is lifted to yield $a_{1u}+e_u$ and $a_{2u}+e_u$ sets, respectively. As concerns the low-lying crystal-field levels in KCeO$_2$, surprisingly large a_{2u}–e_u and a_{2u}–a_{1u} splittings of 96 and 131 meV are computed by MRCI (see Table II). This provides a ground-state spin-orbit wave-function that has significantly stronger contribution, 65%, from the lowest $^2A_{2u}$ trigonal-field term and only ~35% from ^2E_u and $^2A_{1u}$. Since in this way the in-plane a_{2u}–a_{2u} superexchange is enhanced, the result is relevant to the analysis of the effective magnetic couplings (see [38–41] for recent discussion of superexchange paths in rare-earth oxides and chalcogenides).

Having so strong crystal-field effects also gives rise to large excitation energies for the low-lying spin-orbit states — by MRCI+SOC calculations [42], we find that the second and third spin-orbit doublets (relative energies of 121 and 143 meV in Table II) are separated by roughly the same amount from the ground state and from the next excited Kramers doublets. For a free ion, these next excited states are part of the $^2F_{7/2}$ manifold. While degenerate in vacuum, the higher-lying eight spin-orbit states cover an energy window of more than 200 meV in KCeO$_2$. For completeness, we also performed a calculation for a free Ce^{3+} ion, using the same basis sets and quantum chemical program. The $^2F_{5/2}$–$^2F_{7/2}$ splitting is $\Delta_{\mathrm{SOC}}=250$ meV by spin-orbit CASSCF. It implies a spin-orbit coupling constant $\lambda=2\Delta_{\mathrm{SOC}}/7=71$ meV [43], smaller by $\approx$20 meV than the a_{2u}–e_u splitting and by a factor of $\approx$4.4 than the a_{2u}–a'_{2u} splitting in Table II. This λ is actually weaker than the corresponding parameter of, e.g., Ru^{3+} $4d^5$ ions on the Kitaev honeycomb lattice of α-RuCl$_3$ [44, 45].

To put our results in perspective, we note that the lowest two excitation energies (121 and 143 meV, see Table II) are larger by factors of $\gtrsim$4 than the values reported for the Ce $2p$ halide CeF$_3$ [46]. While this can be qualitatively understood on the basis of the larger ligand ionic charges in the oxide, the difference is nevertheless remarkable. Compared to the sulphide KCeS$_2$ [15], the lowest excitation energies are larger by factors of 2–3 in KCeO$_2$, matching the trend pointed out by Gerlinger and Schaack when replacing Cl ($3p$ valence-shell ligand) by F ($2p$ ligand) within the Ce-halide CeX$_3$ family [46].

Interesting as well is that even for an artificial geometry having the six ligands around the reference Ce site shifted along the z coordinate away from the Ce ion such that the CeO$_6$ octahedron is cubic, the second and third spin-orbit doublets are still separated from each other by approximately 20 meV (see Table III). Since for an isolated cubic octahedron the lowest excited f^1 state is a Γ_8 quartet (see, e.g., [35, 37]), this splitting of $\approx$20 meV points to the important role of structural anisotropies beyond the ligand coordination shell, confirming results of earlier studies on either $4f$, $5d$, or $4d$ compounds [9, 32, 47, 48]. The trigonal ligand-cage com-

TABLE III. Ce^{3+} $4f^1$ multiplet structure (relative energies in meV) for an idealized cubic CeO$_6$ octahedron, obtained by appropriately shifting the six ligands along the z coordinate, away from the reference Ce site. The ground-state g factors are $g_c=0.64$ and $g_{ab}=0.10$.

	CASSCF	MRCI	MRCI+SOC	
$^2A_{2u}$	0	0	0	Γ_6
$^2A_{1u}$	37	38	117	Γ_6
^2E_u	122	125	138	$\Gamma_4+\Gamma_5$
	122	125	248	Γ_6
$^2E'_u$	212	215	363	Γ_6
	212	215	375	$\Gamma_4+\Gamma_5$
$^2A'_{2u}$	220	225	425	Γ_6

pression and anisotropies of the extended environment seem in fact to work in opposite directions as concerns the e_u–a_{1u} and e'_u–a'_{2u} splittings: for the cubic octahedron (results in Table III), the a_{1u} level is lower in energy as compared to the e_u states, rather close to the a_{2u} component, while a_{1u} is above e_u with trigonal squeezing of the O$_6$ unit (see Table II); a similar trend is seen for the a'_{2u} level, although the latter does not move below e'_u when the trigonal squeezing is undone. The consequence of a reversed sequence of the e_u and a_{1u} crystal-field levels is an inverted sequence of the lowest two spin-orbit excited states (see also the model-Hamiltonian analysis in Ref. [49]).

Such modulations of the crystal-field splittings, e_u–a_{1u} and a_{2u}–a_{1u}, through (small) ligand displacements are also of interest in the context of electron-lattice couplings, i.e., the interaction between the nonspherical $4f$ electronic cloud and optical phonons. Electron-lattice couplings are known to be strong in Ce compounds (see, e.g., the discussion in Ref. [46]). They were invoked in relation to peculiar features in the Raman spectra of the tysonite trifluoride CeF$_3$ [46] and are more recently discussed as a possible mechanism behind the occurence of low-intensity peaks in inelastic neutron scattering experiments on Ce^{3+} pyrochlores [21].

A related aspect analyzed in Ce^{3+} $4f^1$ pyrochlores is tailoring the e_u–$a_{2u,1u}$ splittings for realizing a $\Gamma_4+\Gamma_5$ on-site spin-orbit ground state, associated with novel multipolar degrees of freedom and new topological characteristics [50? –52]. An *ab initio* study as performed here on the interplay of ligand-cage distortions and anisotropic effects involving surroundings beyond the ligand coordination shell is also of interest for pyrochlore $4f$ compounds since it would better define the conditions under which the $\Gamma_4+\Gamma_5$ ground state can be obtained. Important structural details in pyrochlore Ce^{3+} systems are (i) having two additional ligands on the trigonal axis (the ligand cage is defined by eight O ions in pyrochlores) and (ii) having less pronounced ionic charge imbalance [53] between the two different types of cation species in the immediate neighborhood (formally 4+ transition-

metal and 3+ Ce nearby sites in the pyrochlores vs 3+ Ce and 1+ alkali nearby cations in the delaffosite structure). These structural features in principle destabilize the a_{2u} and a_{1u} orbitals with respect to the e_u components. A $\Gamma_4 + \Gamma_5$ ground state can then be easily envisaged in $4f^1$ pyrochlores but does not seem likely in layered triangular-lattice compounds [54].

We also note that the corrections brought by MRCI to CASSCF are tiny, much less than in the case of $4f^{13}$ delafossites [9]. This can be to large extent understood on the basis of the small number of electrons within the f shell; it also indicates that O-to-Ce charge-transfer effects do not play an important role [37]. Good agreement is therefore expected with experimental data on the on-site f-f excitations, coming from either inelastic neutron scattering or Raman spectroscopy. In the context of growing interest in the research area of $4f$ delafossite-structure quantum magnets, with extensive literature already available on $\tilde{S} = 1/2$ $4f^{13}$ delafossites [3–8], our analysis provides useful *ab initio* benchmarks for the electronic structure of 'complemental' $\tilde{S} = 1/2$ $4f^1$ compounds.

Conclusions. In sum, we present an *ab initio* investigation of the Ce f-shell multiplet structure in the triangular-lattice compound KCeO$_2$. Using atomic positions as obtained by DFT lattice optimization, remarkably large crystal-field splittings are subsequently computed by wave-function-based quantum chemical methods. A regime that appears unusual for f-electron materials is realized this way, in which the splittings among the $4f$ levels as a result of anisotropic surroundings, up to ≈ 320 meV, are larger than both the spin-orbit coupling constant, $\lambda \approx 70$ meV, and characteristic free-ion $^2F_{5/2} - {}^2F_{7/2}$ splitting, $\Delta_{\mathrm{SOC}} = 250$ meV. It remains to be seen how such a setting affects intersite spin interactions, through calculations based on either effective superexchange models [38–41] or on *ab initio* methods [44, 55–58]. Crystal-field splittings as large as the strength of the spin-orbit coupling are also realized under high pressure in, e. g., the $4d^5$ Kitaev honeycomb compound α-RuCl$_3$; by modifying the composition of the ground-state wavefunction and the dominant exchange paths, they favor Heisenberg antiferromagnetism in that case [14]. Such findings in $4d^5$ materials suggest that KCeO$_2$ is an interesting model system in the $4f^1$ category.

[1] Y. Li, H. Liao, Z. Zhang, S. Li, F. Jin, L. Ling, L. Zhang, Y. Zou, L. Pi, Z. Yang, J. Wang, Z. Wu, and Q. Zhang, "Gapless quantum spin liquid ground state in the two-dimensional spin-1/2 triangular antiferromagnet ybmggao$_4$," Sci. Rep. **5**, 16419 (2015).

[2] Y. Li, G. Chen, W. Tong, L. Pi, J. Liu, Z. Yang, X. Wang, and Q. Zhang, "Rare-earth triangular lattice spin liquid: A single-crystal study of ybmggao$_4$," Phys. Rev. Lett. **115**, 167203 (2015).

[3] W Liu, Z Zhang, J Ji, Y Liu, J Li, H Lei, and Q Zhang, "Rare-earth chalcogenides: A large family of triangular lattice spin liquid candidates," Chin. Phys. Lett. **35**, 117501 (2018).

[4] M Baenitz, Ph Schlender, J Sichelschmidt, Y A Onykiienko, Z Zangeneh, K M Ranjith, R Sarkar, L Hozoi, H C Walker, J-C Orain, H Yasuoka, J van den Brink, H H Klauss, D S Inosov, and Th. Doert, "Frustration and anisotropic exchange in ytterbium magnets with edge-shared octahedra," Phys. Rev. B **98**, 220409 (2018).

[5] K. M. Ranjith, D. Dmytriieva, S. Khim, J. Sichelschmidt, S. Luther, D. Ehlers, H. Yasuoka, J. Wosnitza, A. A. Tsirlin, H. Kühne, and M. Baenitz, "Field-induced instability of the quantum-spin-liquid ground state in the j=1/2 triangular-lattice compound naybo$_2$," Phys. Rev. B **99**, 180401 (2019).

[6] L. Ding, M. Pascal, S. Bachus, F. Grußler, P. Gegenwart, J. Singleton, R. D. Johnson, H. C. Walker, D. T. Adroja, A. D. Hillier, and A. A. Tsirlin, "Gapless spin-liquid state in the structurally disorder-free triangular antiferromagnet nayb$_2$," Phys. Rev. B **100**, 144432 (2019).

[7] M. Bordelon, E. Kenney, T. Hogan, L. Posthuma, M. Kavand, Y. Lyu, M. Sherwin, C. Brown, M. J. Graf, L. Balents, and S. D. Wilson, "Field-tunable quantum disordered ground state in the triangular lattice antiferromagnet nayb$_2$," Nat. Phys. **15**, 1058 (2019).

[8] P-L Dai, G Zhang, Y Xie, C Duan, Y Gao, Z Zhu, E Feng, C-L Huang, H Cao, A Podlesnyak, G E Granroth, D Voneshen, S Wang, G Tan, E Morosan, X Wang, L Shu, G Chen, Y Guo, X Lu, and P Dai, "Spinon fermi surface spin liquid in a triangular lattice antiferromagnet naybse$_2$," arXiv:2004.06867 (2020).

[9] Z Zangeneh, S Avdoshenko, J van den Brink, and L Hozoi, "Single-site magnetic anisotropy governed by interlayer cation charge imbalance in triangular-lattice aybx$_2$," Phys. Rev. B **100**, 174436 (2019).

[10] R Clos, M Devalette, C Fouassier, and P Hagenmuller, Mat. Res. Bull. **5**, 179 (1970).

[11] D Aravena, M Atanasov, and F Neese, "Periodic trends in lanthanide compounds through the eyes of multireference ab initio theory," Inorg. Chem. **55**, 4457 (2016).

[12] N. A. Bogdanov, V. M. Katukuri, H. Stoll, J. van den Brink, and L. Hozoi, "Post-perovskite CaIrO$_3$: A j=1/2 quasi-one-dimensional antiferromagnet," Phys. Rev. B **85**, 235147 (2012).

[13] M. Moretti Sala, S. Boseggia, D. F. McMorrow, and G. Monaco, "Resonant X-Ray Scattering and the $j_{\mathrm{eff}}=1/2$ Electronic Ground State in Iridate Perovskites," Phys. Rev. Lett. **112**, 026403 (2014).

[14] G. Bastien, G. Garbarino, R. Yadav, F. J. Martinez-Casado, R. Beltrán-Rodríguez, Q. Stahl, M. Kusch, S. P. Limandri, R. Ray, P. Lampen-Kelley, D. G. Mandrus, S. E. Nagler, M. Roslova, A. Isaeva, T. Doert, L. Hozoi, A. U. B. Wolter, B. Büchner, J. Geck, and J. van den Brink, "Pressure-induced dimerization and valence bond crystal formation in the kitaev-heisenberg magnet rucl3," Phys. Rev. B **97**, 241108(R) (2018).

[15] G Bastien, B Rubrecht, E Haeussler, P Schlender, Z Zangeneh, S Avdoshenko, R Sarkar, A Alfonsov, S Luther, Y A Onykiienko, H C Walker, H Kühne, V Grinenko, Z Guguchia, V Kataev, H-H Klauss, L Hozoi, J van den Brink, D S Inosov, B Büchner, A U B Wolter, and T Doert, "Long-range magnetic order in the s=1/2 triangular lattice antiferromagnet kces$_2$," SciPost Phys. **9**, 041 (2020).

[16] Klaus Koepernik and Helmut Eschrig, "Full-potential nonorthogonal local-orbital minimum-basis band-structure scheme," Phys. Rev. B **59**, 1743–1757 (1999).

[17] John P. Perdew, Kieron Burke, and Matthias Ernzerhof, "Generalized gradient approximation made simple," Phys. Rev. Lett. **77**, 3865–3868 (1996).

[18] Mayukh Majumder, Gediminas Simutis, Ines E Collings, Jean-Christophe Orain, Tusharkanti Dey, Yuesheng Li, Philipp Gegenwart, and Alexander A. Tsirlin, "Persistent spin dynamics in the pressurized spin-liquid candidate ybmggao$_4$," Phys. Rev. Research **2**, 023191 (2020).

[19] Joseph B Mann, *Atomic structure calculations. I. Hartree–Fock energy results for the elements hydrogen to lawrencium*, Tech. Rep. (Los Alamos Scientific Lab., N. Mex., 1967).

[20] B. G. Wybourne, *Spectroscopic properties of rare earths* (Interscience Publishers, New York, 1965).

[21] J. Gaudet, E. M. Smith, J. Dudemaine, J. Beare, C. R. C. Buhariwalla, N. P. Butch, M. B. Stone, A. I. Kolesnikov, G Xu, D. R. Yahne, K. A. Ross, C. A. Marjerrison, J. D. Garrett, G. M. Luke, A. D. Bianchi, and B. D. Gaulin, "Quantum spin ice dynamics in the dipole-octupole pyrochlore magnet ce$_2$zr$_2$o$_7$," Phys. Rev. Lett. **122**, 187201 (2019).

[22] T. Helgaker, P. Jørgensen, and J. Olsen, *Molecular Electronic-Structure Theory* (Wiley, Chichester, 2000).

[23] P. J. Knowles and H.-J. Werner, "Internally contracted multiconfiguration-reference configuration interaction calculations for excited states," Theor. Chim. Acta **84**, 95–103 (1992).

[24] M. Dolg, H. Stoll, and H. Preuss, J. Chem. Phys. **90**, 1730 (1989).

[25] X. Cao and M. Dolg, J. Mol. Struct. (Theochem) **581**, 139 (2002).

[26] W. A. de Jong, R. J. Harrison, and D. A. Dixon, J. Chem. Phys. **114**, 48 (2001).

[27] M. Dolg, H. Stoll, A. Savin, and H. Preuss, Theor. Chim. Acta **75**, 173 (1989).

[28] M. Dolg, H. Stoll, and H. Preuss, Theor. Chim. Acta **85**, 441 (1993).

[29] P. Fuentealba, H. Preuss, H. Stoll, and L. von Szentpaly, Chem. Phys. Lett. **89**, 418 (1982).

[30] M. Klintenberg, S. E. Derenzo, and M. J. Weber, Comput. Phys. Commun. **131**, 120 (2000).

[31] I Kebaili and M Dammak, J. Theor. Appl. Phys. **6**, 21 (2012).

[32] N. A. Bogdanov, V. M. Katukuri, J. Romhányi, V. Yushankhai, V. Kataev, B. Büchner, J. van den Brink, and L. Hozoi, "Orbital reconstruction in nonpolar tetravalent transition-metal oxide layers," Nat. Commun. **6**, 7306 (2015).

[33] H. J. Werner, P. J. Knowles, G. Knizia, F. R. Manby, and M. Schütz, "Molpro: a general-purpose quantum chemistry program package," Wiley Rev: Comp. Mol. Sci. **2**, 242–253 (2012).

[34] S. Sugano, Y. Tanabe, and H. Kamimura, *Multiplets of Transition-Metal Ions in Crystals* (Academic Press, New York, 1970).

[35] J S Griffith and L E Orgel, J. Chem. Phys. **26**, 988 (1957).

[36] There are rather detailed studies providing estimates for the a_{2u}–t_{2u} splitting in Ce halides with O_h symmetry, see e.g. Table 3 in Ref. [37] and Fig. S1 in Ref. [11]. It implies a scale of ∼30 meV according to *ab initio* data reported in Ref. [11].

[37] W W Lukens, N M Edelstein, N Magnani, T W Hayton, S Fortier, and L A Seaman, "Quantifying the σ and π interactions between u(v) f orbitals and halide, alkyl, alkoxide, amide and ketimide ligands," J. Am. Chem. Soc. **135**, 10742 (2013).

[38] V S Mironov, J. Phys.: Condens. Matter **8**, 10551 (1996).

[39] A V Palii, Mold. J. Phys. Sci. **2**, 291 (2003).

[40] J G Rau and M J P Gingras, "Frustration and anisotropic exchange in ytterbium magnets with edge-shared octahedra," Phys. Rev. B **98**, 054408 (2018).

[41] Y Motome, R Sano, S Jang, Y Sugita, and Y Kato, "Materials design of kitaev spin liquids beyond the jackeli-khaliullin mechanism," J. Phys.: Condens. Matter **32**, 404001 (2020).

[42] A. Berning, M. Schweizer, H.-J. Werner, P. J. Knowles, and P. Palmieri, "Spin-orbit matrix elements for internally contracted multireference configuration interaction wavefunctions," Mol. Phys. **98**, 1823–1833 (2000).

[43] Somewhat smaller than estimates for Ce halides [11].

[44] R. Yadav, N. A. Bogdanov, V. M. Katukuri, S. Nishimoto, J. van den Brink, and L. Hozoi, "Kitaev exchange and field-induced quantum spin-liquid states in honeycomb α-RuCl$_3$," Sci. Rep. **6**, 37925 (2016).

[45] P Warzanowski, N Borgwardt, K Hopfer, J Attig, T C Koethe, P Becker, V Tsurkan, A Loidl, M Hermanns, P H M van Loosdrecht, and M Grüninger, "Multiple spin-orbit excitons and the electronic structure of α-rucl$_3$," Phys. Rev. Research **2**, 042007(R) (2020).

[46] H Gerlinger and G Schaack, Phys. Rev. B **33**, 7438 (1986).

[47] V. M. Katukuri, K. Roszeitis, V. Yushankhai, A. Mitrushchenkov, H. Stoll, M. van Veenendaal, P. Fulde, J. van den Brink, and L. Hozoi, "Electronic structure of low-dimensional 4d^5 oxides: interplay of ligand distortions, overall lattice anisotropy, and spin-orbit interactions," Inorg. Chem. **53**, 4833 (2014).

[48] N. A. Bogdanov, R. Maurice, I. Rousochatzakis, J. van den Brink, and L. Hozoi, "Magnetic state of pyrochlore Cd$_2$Os$_2$O$_7$ emerging from strong competition of ligand distortions and longer-range crystalline anisotropy," Phys. Rev. Lett. **110**, 127206 (2013).

[49] W G Perkins and G A Crosby, J. Chem. Phys. **42**, 407 (1965).

[50] Yi-Ping Huang, Gang Chen, and Michael Hermele, "Quantum spin ices and topological phases from dipolar-octupolar doublets on the pyrochlore lattice," Phys. Rev. Lett. **112**, 167203 (2014).

[51] Y-D Li and G Chen, "Symmetry enriched u(1) topological orders for dipole-octupole doublets on a pyrochlore lattice," Phys. Rev. B **95**, 041106(R) (2017).

[52] D S Inosov, "Ice of higher order," Nat. Phys. **16**, 507 (2020).

[53] This is a main aspect discussed in, e.g., Refs. [9, 48].

[54] Y-D Li, X Wang, and G Chen, "Hidden multipolar orders of dipole-octupole doublets on a triangular lattice," Phys. Rev. B **94**, 201114(R) (2016).

[55] V. M. Katukuri, S. Nishimoto, V. Yushankhai, A. Stoyanova, H. Kandpal, S. Choi, R. Coldea, I. Rousochatzakis, L. Hozoi, and J. van den Brink, "Kitaev interactions between $J = 1/2$ moments in honeycomb Na_2IrO_3 are large and ferromagnetic: Insights from *ab initio* quantum chemistry calculations," New J. Phys. **16**, 013056 (2014).

[56] N Iwahara and L F Chibotaru, "Exchange interaction between J multiplets," Phys. Rev. B **91**, 174438 (2015).

[57] F Gendron, J Autschbach, J-P Malrieu, and H Bolvin, "Magnetic coupling in the ce(iii) dimer $ce_2(cot)_3$," Inorg. Chem. **58**, 581 (2019).

[58] P P Hallmen, H-J Werner, D Kats, S Lenz, G Rauhut, H Stoll, and J van Slageren, "Toward fast and accurate ab initio calcu of magnetic exchange in polynuclear lanthanide complexes," Phys. Chem. Chem. Phys **21**, 9769 (2019).

This figure "fig_cryst_struct_jun07.png" is available in "png" format from:

http://arxiv.org/ps/2012.13174v1

This figure "DOS_Partials_GGA_Fig_abc_aug31.png" is available in "png" format f

http://arxiv.org/ps/2012.13174v1